M. Selva[1,*], L. Santurri and S. Baronti, "**Improving Hypersharpening for WorldView-3 Data**," in IEEE Geoscience and Remote Sensing Letters, vol. 16, no. 6, pp. 987-991, June 2019, doi: 10.1109/LGRS.2018.2884087.

The published version of the paper can be downloaded from IEEE *Xplore*® at this link:
https://ieeexplore.ieee.org/abstract/document/8584412

[1] "Nello Carrara" Institute of Applied Physics, National Research Council, 50019 Sesto Fiorentino (FI), Italy.
* Correspondence: m.selva@ifac.cnr.it

**To cite this paper:**

M. Selva, L. Santurri and S. Baronti, "Improving Hypersharpening for WorldView-3 Data," in IEEE Geoscience and Remote Sensing Letters, vol. 16, no. 6, pp. 987-991, June 2019, doi: 10.1109/LGRS.2018.2884087.

```
@ARTICLE{8584412,
  author={Selva, Massimo and Santurri, Leonardo and Baronti, Stefano},
  journal={IEEE Geoscience and Remote Sensing Letters},
  title={Improving Hypersharpening for WorldView-3 Data},
  year={2019},
  volume={16},
  number={6},
  pages={987-991},
  doi={10.1109/LGRS.2018.2884087}}
```

# Improving Hypersharpening for WorldView-3 Data

Massimo Selva, Leonardo Santurri and Stefano Baronti *Member IEEE*

***Abstract*—In this letter hypersharpening is analyzed in depth by investigating some weaknesses present in its formulation. It is shown that the key formula of the synthesized band variant can be simplified under certain circumstances.**

**In addition, a novel fusion schema is proposed. As a result, the gain factor adopted to weight the injected detail, is computed in a different way.**

**This schema can be applied to fuse a wide range of hyperspectral and multispectral data. In this letter, its effectiveness is demonstrated by taking into account the characteristics of WorldView-3 data.**

***Index Terms*—Hypersharpening, Image Fusion, Pansharpening, Remote Sensing, WorldView-3.**

## I. Introduction

*Hypersharpening* was introduced at WHISPERS 2014 [1] and has been theoretically developed in [2].

As technological developments are replacing or complementing panchromatic (Pan) cameras with multispectral (MS) and hyperspectral (HS) instruments, the term pansharpening is no longer suitable for indicating the fusion methods that spatially enhance MS/HS data sets.

Pansharpening, in fact, implies the existence of only *one single* image at a high spatial resolution suitable for enhancing the sharpness of some MS/HS bands acquired at a lower resolution. The term *hypersharpening* points out that the spatial source, which was previously *one single* image (panchromatic), can be *a set* (potentially a *hyperspectral cube*) of bands.

The first step from pansharpening towards hypersharpening was induced by launching the Earth Observer 1 (EO-1) satellite in 2000. EO-1, in fact, hosted the Advanced Land Imager (ALI) MS + Pan scanner and the Hyperion imaging HS spectrometer. The swaths of ALI and Hyperion were partially overlapped, in such a way that there was a part of the acquired area in which Pan, MS and HS data were simultaneously available.

In particular, it was possible to develop and apply fusion algorithms in order to spatially enhance a HS image for a 3:1 scale ratio, thus extending pansharpening to HS data.

In this perspective, HS resolution enhancement, or HS sharpening, refers to the processing of the data in order to synthesize an HS product that ideally exhibits the spectral characteristics of the original HS image at the higher spatial resolution.

Even though many developments of spatial resolution enhancement of HS data have been rough extensions of MS pansharpening algorithms [3], also specific approaches have been proposed in the literature.

For example in [4], a maximum a posteriori (MAP) estimation method was introduced. The MAP estimation was based on a spatially-varying statistical model to enhance the HS image resolution. This Bayesian approach was further improved by the same authors in [5] where they investigated and demonstrated the advantages of using a high-resolution MS image as the source for a MS/HS fusion. In this way, the concept of hypersharpening was implicitly introduced.

The hypersharpening approach proposed in [6] which is based on [4], works in the wavelet domain and assumes a joint normal model for the images and an additive noise-imaging model for the HS data. This approach, however, is time-consuming.

Subsequently, the approach presented in [7] was based on a linear spectral mixture model and implemented using coupled non-negative matrix factorization (CNMF) unmixing. Sensor observation models that relate the two data sets were built into the initialization matrix of each NMF unmixing procedure. This method is physically straightforward, but computationally expensive and not very intuitive. This particular approach was experimented on Hyperspectral Imager Suite (HISUI) simulated data [8].

Interesting hypersharpening methods have been developed more recently. In [9], the authors propose a hypersharpening approach that builds a Bayesian fusion model by taking into account constraints related to the fusion problem via an appropriate prior distribution. In [10], hypersharpening is considered as an inverse problem. Data fusion is based on the minimization of a convex objective function containing two quadratic data-fitting terms and an edge-preserving regularizer. Unfortunately, all the methods discussed so far suffer from a high computational complexity that necessitates the processing of small images.

In [2], hypersharpening considers the characteristics of the data acquired by SIM-GA. This instrument, which was developed by Leonardo S.p.A., consists of a panchromatic camera and two hyperspectral sensors in the VNIR and SWIR spectral ranges, respectively. The resolution factor is roughly 3 between Pan and the VNIR spectrometer and is again 3 between the VNIR and SWIR spectrometers as well. Therefore hypersharpening, by using VNIR hyperspectral data, can perform the spatial enhancement of SWIR.

The acquisition of multi-sensors, multi-resolutions data of

The work was developed within the framework of the SMART (Spettrometro Miniaturizzato Avanzato per Ricerca Tecnologica) project, supported by POR - FESR 2014-2020 and funded by the Tuscan Region.

M. Selva, L. Santurri and S. Baronti are employed at the "Nello Carrara" Institute of Applied Physics, National Research Council, Florence Research Area, 50019 Sesto Fiorentino (FI), Italy (e-mail: {m.selva l.santurri s.baronti }@ifac.cnr.it).

the same area is, in fact, a key aspect of state-of-the-art satellite technology.

The WorldView-3 satellite (launched by DigitalGlobe on 13 August 2014 ) and the Sentinel-2 satellite (launched by ESA on 23 June 2015) really exhibit this capability. Therefore, hypersharpening framework can be applied to data acquired by these two satellites.

In [11], in fact, four different approaches are discussed for generating WorldView-3 HR SWIR images from VNIR data. Such approaches are combinations of pansharpening and hypersharpening methods. In the paper a new picture quality predictor that does not need a reference image for assessing hypersharpening performance is also proposed.

As regards Sentinel-2, in [12] a hypersharpening methodology, known as SMUSH, is proposed. It is a hierarchical method based on an optimization approach. The objective function contains a quadratic data fitting term, an edge preserving regularizer and a patch-based plug-and-play prior-promoting self-similar image.

Inspired by the success of deep learning in image enhancement, a hypersharpening approach is proposed in [13] by designing a deep convolutional neural network (CNN) with two branches that are devoted to features of hyperspectral and multispectral images, respectively. This methodology is experimented by fusing Hyperion and Sentinel-2 data.

An extensive up-to-date review of hypersharpening and pansharpening methodologies can be found in [14].

In the remain part of this letter, new developments on hypersharpening are presented. Some basic points of hypersharpening are discussed by considering the formulation proposed in [2]. The analysis identifies a variant for computing the injection gain of the spatial details. Its effectiveness is demonstrated on WorldView-3 simulated data.

The theory of hypersharpening is recalled in Section II. New developments are presented in Section III. Section IV is devoted to introducing the dataset adopted for tests, while results are presented and discussed in V. Conclusions are drawn in Section VI.

## II. Hypersharpening

Let the symbol **HS** be used to indicate the original high spatial resolution hyperspectral data set. The symbol **hs** indicates the original low-resolution spatial hyperspectral data set. $M$ and $N$ represent the numbers of bands of **HS** and **hs**, respectively. Thus, let the following be defined:

- $\mathbf{hs} \triangleq \{hs_n, \quad n = 1, \ldots, N\}$ as the original low resolution hyperspectral image.
- $\mathbf{hs}_{exp} \triangleq \{hs_{n_{exp}}, \quad n = 1, \ldots, N\}$ as the **hs** image interpolated at full scale.
- $\hat{\mathbf{hs}} \triangleq \{\hat{hs}_n, \quad n = 1, \ldots, N\}$ as the fused **hs** image.
- $\mathbf{HS} \triangleq \{HS_m, \quad m = 1, \ldots, M\}$ as the original high-resolution hyperspectral image.
- $\tilde{\mathbf{HS}} \triangleq \{\tilde{HS}_m, \quad m = 1, \ldots, M\}$ as **HS** at the degraded scale and obtained by low-pass filtering and downsampling each $HS_m$ band.
- $\tilde{\mathbf{HS}}_{exp} \triangleq \{\tilde{HS}_{m_{exp}}, \quad m = 1, \ldots, M\}$ as $\tilde{\mathbf{HS}}$ interpolated at full scale.

According to the previous definitions, the spatial detail $D_m$ of $HS_m$ is given by:

$$D_m = HS_m - \tilde{HS}_{m_{exp}} \tag{1}$$

The symbol $X_n$ is now introduced to indicate the band that will be derived from **HS**. $X_n$ is, for each band $hs_n$, the source of spatial detail from which to obtain the fused band $\hat{hs}_n$. **X** is the hyperspectral set constituted by all these bands. In conventional pansharpening, $X_n$ is always the panchromatic $P$, but, in the hypersharpening approach, it can be any band or any weighted modeling of the high-spatial resolution bands of **HS**. Furthermore, $X_n$ can be defined according to any reasonable criterion, thus giving a further degree of freedom to fusion algorithms. According to the previous notation, the following symbols are defined:

- $\tilde{X}_n$ as the band $X_n$ lowpass filtered and downsampled at degraded scale.
- $\tilde{X}_{n_{exp}}$ as the $\tilde{X}_n$ band interpolated at full scale.
- $S_n$ as the the spatial detail of $X_n$.

The following relationship holds:

$$S_n = X_n - \tilde{X}_{n_{exp}} \tag{2}$$

According to the definitions of $X_n$ and $S_n$, the fusion schema discussed in [2] is:

$$\hat{hs}_n \triangleq hs_{n_{exp}} + g_n \cdot S_n \tag{3}$$

where $g_n$ is a gain factor that may be constant for each pixel in the band or computed locally. In [2], $g_n$ is global and defined as:

$$g_n = \frac{cov(hs_{n_{exp}}, \tilde{X}_{n_{exp}})}{\sigma^2_{\tilde{X}_{n_{exp}}}} \tag{4}$$

where the symbol $cov()$ indicates the covariance and $\sigma^2$ the variance of the referred entities.

Eq. (3) shows that each fused band is obtained by adding to the expanded band the weighted difference between the high spatial resolution source $X_n$ and the band $X_n$ itself, first reduced at degraded scale and then expanded at full scale.

In [2] two variants were proposed.

The former, *Selected band*, consists simply of using a single band $HS_{\bar{m}}$ as $X_n$, where $\bar{m}$ is given by:

$$\bar{m} = \arg\max_m corr(hs_{n_{exp}}, \tilde{HS}_{m_{exp}}) \tag{5}$$

that is, $HS_{\bar{m}}$ is the band that, once degraded and expanded at full scale, exhibits the highest correlation value with $hs_{n_{exp}}$.

The latter *Synthesized band* estimates a set of coefficients $w_{n_1}, \ldots w_{n_l}, \ldots w_{n_M}$ for each $hs_n$ by means of a linear regression algorithm, in order to minimize the MSE between $hs_{n_{exp}}$ and the linear combination of the bands $\{\tilde{HS}_{m_{exp}}\}$ over all the pixels of the band. After the estimation of the set of regression coefficients, assuming that these coefficients are a valid estimation also at full resolution as discussed in [15], $X_n$ is synthesized according to:

$$X_n = \sum_{m=1}^{M} w_{n_m} \cdot HS_m \tag{6}$$

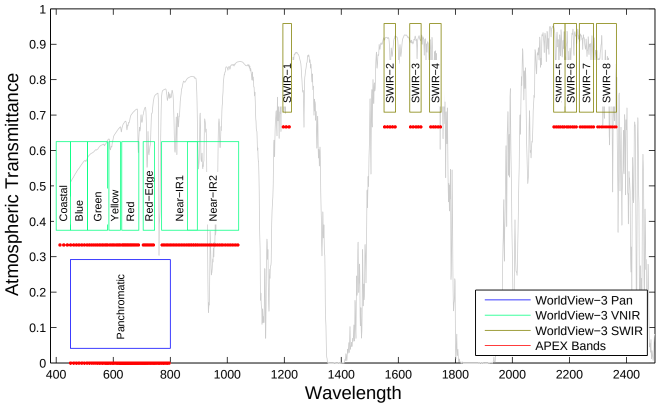


Figure 1: Spectral ranges of WorldView-3 bands.

Considering now (1), (2) and that

$$\tilde{X}_{n_{exp}} = \sum_{m=1}^{M} w_{n_m} \cdot \tilde{HS}_{m_{exp}} \tag{7}$$

the following relationships hold:

$$S_n = \sum_{m=1}^{M} w_{n_m} \cdot D_m \tag{8}$$

## III. Hypersharpening: New Developments

When hypersharpening was developed, since the traditional work flow of pansharpening was considered effective, a great attention was devoted only to how to obtain $X_n$. In other words, hypersharpening was defined by computing $X_n$ before applying the traditional pansharpening expressed by (3). Thus, any problems that could have arisen from how $X_n$ was computed and (3) were ignored.

Let the gain formula (4) be expressed as:

$$g_n = t_{1_n} \cdot t_{2_n} \tag{9}$$

where $t_{1_n}$ and $t_{2_n}$ terms are defined as:

$$t_{1_n} = corr(hs_{n_{exp}}, \tilde{X}_{n_{exp}}) \tag{10}$$

$$t_{2_n} = \frac{\sigma_{hs_{n_{exp}}}}{\sigma_{\tilde{X}_{n_{exp}}}} \tag{11}$$

where the symbol $corr()$ indicates the correlation operation. In the Synthesized band variant, the minimization between $hs_{n_{exp}}$ and the linear combination of the bands $\{\tilde{HS}_{m_{exp}}\}$ implies that $\tilde{X}_{n_{exp}}$ is similar to $hs_{n_{exp}}$ as far as this is possible. Consequently, since both terms $t_{1_n}$ and $t_{2_n}$ tend to 1, also the $g_n$ injection gain tends to 1.

On the other hand, the minimization of the MSE between the linear combination of the bands $\{\tilde{HS}_{m_{exp}}\}$ and $hs_{n_{exp}}$ does not automatically implies that $g_n$ is equal to 1.

When $g_n \simeq 1$, i.e. when the minimization is particulary effective, the synthesized band variant hides a paradox: the gain term has no influence on the fusion results.

This fact determines the important consequence that (3) can be simplified as:

$$\hat{hs}_n = hs_{n_{exp}} + S_n \tag{12}$$

| | Pan | VNIR | SWIR |
|---|---|---|---|
| Spectral range | $450-800$ nm | $400-1040$ nm | $1195-2365$ nm |
| Spectral bands | 1 | 8 | 8 |
| GSD @ Nadir | 0.31 m | 1.24 m | 3.70 m |

Table I: Characteristics of the WorldView-3 data.

| | |
|---|---|
| Spectral coverage | $413-2421$ nm |
| Bands | 285 |
| Dimensions ($h \times w$) | $1500 \times 1000$ |
| Pixel Size | 1.8 m |
| Date of the acquisition | 2011-06-26 |

Table II: Characteristics of the APEX dataset adopted.

Since $\tilde{X}_{n_{exp}}$ does not appear in (12), computing (7) is useless and (8) is the only equation needed for performing fusion. Thus, the *Synthesized band* variant is really a *Synthesized detail* variant.

Going deeper into the analysis, other important considerations can be made. Even though the MSE minimization determines the $w_{n_m}$ weights used to synthesize $\tilde{X}_{n_{exp}}$ and $S_n$ in (7) and (8) respectively, only the term $S_n$ is directly present in (3).

Therefore $\tilde{X}_{n_{exp}}$ could not be the best choice for processing the gain term of (3). Thus, the MSE constraint could be relaxed in favor of other criteria that could be more effective in increasing the performance of hypersharpening.

The criterion proposed here is that the energy of $\tilde{X}_{n_{exp}}$ and $hs_{n_{exp}}$ should be the same. This can be achieved by matching the histograms of the two bands, thus obtaining a more realistic band $\tilde{X}'_{n_{exp}}$:

$$\tilde{X}'_{n_{exp}} = (\ \tilde{X}_{n_{exp}} - \mu_{\tilde{X}_{n_{exp}}}\ ) \frac{\sigma_{hs_{n_{exp}}}}{\sigma_{\tilde{X}_{n_{exp}}}} + \mu_{hs_{n_{exp}}} \tag{13}$$

where the symbol $\mu$ is the mean of the corresponding band.

The effectiveness of (13) is satisfactory. Readers interested in recent approaches to histogram matching can refer to [16].

By replacing $\tilde{X}_{n_{exp}}$ with $\tilde{X}'_{n_{exp}}$ in (9) and computing the gain accordingly, the fusion formula becomes:

$$\hat{hs}_n = hs_{n_{exp}} + t_{1_n} \cdot S_n \tag{14}$$

The next section demonstrates that (14) is an effective variant in determining an improvement in fusion performances.

## IV. Experiments

One of the goals of this letter is to demonstrate the effectiveness of the proposed hypersharpening variant in fusing WorldView-3 data. WorldView-3 is technologically advanced since it is the first multi-payload, super-spectral, high-resolution commercial satellite sensor. Some of its characteristics are highlighted in Fig. 1 and are reported in Table I. Even if the SWIR spectrometer exhibits a spatial resolution of 3.70 m at Nadir, the SWIR data are resampled and distributed with a sampling spatial interval of 7.5 m. In any case, the hypersharpening framework can be applied to SWIR data (**hs**) by using VNIR data (**HS**) as the source of the high spatial frequencies.

Unfortunately, when real data are processed, the reference is not available and the assessment of the fused images can be carried out only by visual evaluation or by adopting quality indexes that do not require the reference. However, these indices introduce a certain degree of uncertainty into the analysis. Another viable solution for overcoming this limit consists of degrading all the data set to a lower scale and using the original dataset as the reference. This approach is based on the implicit assumption that evaluations at lower scale are also valid at full scale, as discussed in [17]. Thus, applying this strategy to WorldView-3 data would require fusing images from the resolution of 22.5 m to 7.5 m. Consequently, exploiting the capabilities given by the high spatial resolution of WorldView-3 data would be questionable and scarcely significant.

Therefore, in this letter, a different approach has been adopted. WorldView-3 multispectral and panchromatic images have been simulated starting from the APEX hyperspectral open science data set [18]. The characteristics of the APEX data set are reported in Table II. The acquired scene contains areas of forest, agriculture, urban and freshwater and is thus suitable for assessing the fusion methodologies.

Each WorldView-3 band is simulated by weighting the reflectance values of the APEX bands that are contained in the corresponding spectral range. A Gaussian-shaped filter kernel with cut-off value of 0.25 at the Nyquist frequency is adopted for spatial degrading. Thus, a plausible system modulation transfer functions (MTF) is modelled [19]. An interesting discussion regarding the MTF in the pansharpening/hypersharpening field can be found in [20].

Fig. 1, which reports the spectral width of WorldView-3 bands and the central wavelengths of the APEX bands (red points) used for spectral synthesis, well expresses how the simulation data set is created. In Fig. 1, also the atmospheric transmittance is plotted (gray line), for the sake of completeness.

Since APEX hyperspectral data have spatial resolution of 1.8 m, the fusion from 3.7 m to 1.24 m can not be simulated. Therefore, the hypersharpening of the WorldView-3 data is simulated by fusing SWIR at the spatial resolution of 5.4 m with VNIR at 1.8 m. This loss of spatial resolution is assumed to be still acceptable for the analysis. Clearly, the SWIR data at 1.8 m is the reference necessary to assess the fused images.

To complete the analysis, also pansharpening is experimented. The algorithm adopted is equivalent to (3), just as in [2]. In addition, in the flavour of [21] also the SWIR expanded image is taken into account.

## V. Results

In the experiments, the universal image quality index (UIQI) [22] is adopted for spatial quality, the erreur relative globale adimensionnelle de synthèse (ERGAS) [23] for radiometric quality and the spectral angle mapper (SAM) index for spectral quality. The UIQI values are averaged on the 8 SWIR bands.

To assess the effectiveness of the proposed variant, two specific scenarios are reported: urban and vegetation. Accordingly, two sub-images of $480 \times 480$ pixels are identified in the acquired scene and highlighted in Fig. 2 by using a blue and red frame, respectively.

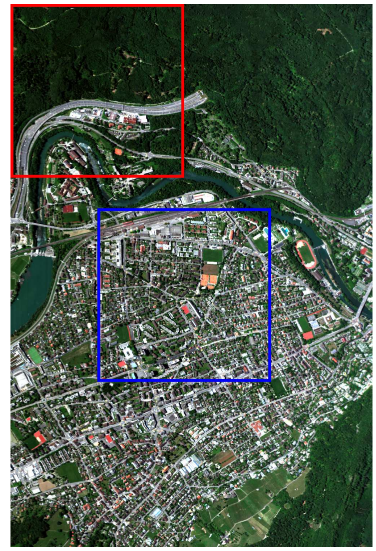

Figure 2: APEX acquired area. The red and blue frames identify the vegetated and urban sub-images, respectively.

Figs 3 and 4 show two specific details of the two sub-images processed; the RGB images are obtained by using the SWIR-1, SWIR-3 and SWIR-8 as red, green and blue channels, respectively. Tables III and IV report the values of the indices computed on the sub-images.

Pansharpening [Figs 3(c)] and hypersharpening selected band [Figs 3(d)] inject unrealistic details on the urban area. These details are absent in the synthesized variant but this image is overly sharp [Figs 3(e)]. The improved synthesized variant determines an image that is more natural and the injected details appears to be of good quality [Figs 3(f)].

As far as the indices are concerned [Table III], the improved synthesized variant presents the best scores. The improvements are particularly relevant for ERGAS and SAM indexes.

As regards the vegetated area, even though Table IV shows that improved synthesized is the best fusion approach, a visual inspection barely made a distinction between the different images [Fig. 4]. When carefully comparing selected and improved synthesized variant, in the latter some details are sharper and the color fidelity appears to be better.

## VI. Conclusions

This letter discusses relevant issues concealed in the previous formulation of hypersharpening, thus opening up interesting research perspectives. The novel fusion schema introduces the histogram matching operation into the synthesized band variant. As a result, the formula of the gain is different from the original one.

The effectiveness of the proposed solution is demonstrated on WorldView-3 simulated data. The novelty introduced is applicable for fusing hyperspectral and multispectral data in general.

## References

[1] M. Selva, B. Aiazzi, F. Butera, L. Chiarantini, and S. Baronti, "Hyper-sharpening of hyperspectral data: A first approach," in *2014 6th Workshop on Hyperspectral Image and Signal Processing: Evolution in Remote Sensing (WHISPERS)*, June 2014, pp. 1–4.

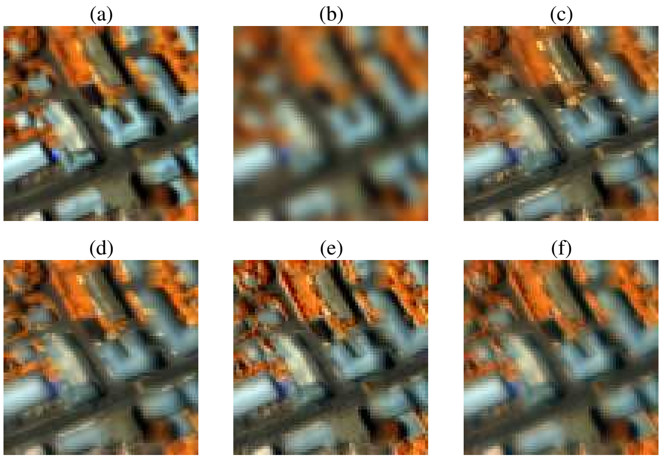


Figure 3: (a) Reference. (b) Expanded Multispectral. (c) Pansharpening. (d) Hypersharpening Selected. (e) Hypersharpening Synthesized. (f) Improved Hypersharpening Synthesized. A specific urban area of 64 × 64 pixels at 1.8 m scale is shown.

| | SAM | ERGAS | $UIQI_{avg}$ |
|---|---|---|---|
| Expanded Multispectral | 3.775 | 7.990 | 0.833 |
| Pansharpening | 3.881 | 7.371 | 0.876 |
| Hypersharpening Selected | 3.632 | 6.999 | 0.892 |
| Hypersharpening Synthesized | 5.489 | 8.891 | 0.852 |
| Improved Hypersharpening Synthesized | **3.623** | **6.781** | **0.898** |

Table III: Quality indices of the urban sub-image.

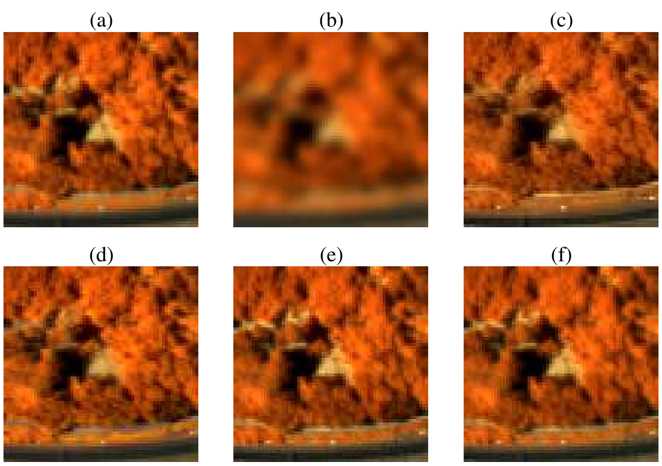


Figure 4: (a) Reference. (b) Expanded Multispectral. (c) Pansharpening. (d) Hypersharpening Selected. (e) Hypersharpening Synthesized. (f) Improved Hypersharpening Synthesized. A specific vegetated area of 64 × 64 pixels at 1.8 m scale is shown.

| | SAM | ERGAS | $UIQI_{avg}$ |
|---|---|---|---|
| Expanded Multispectral | **2.176** | 8.158 | 0.823 |
| Pansharpening | 4.093 | 8.736 | 0.840 |
| Hypersharpening Selected | 4.143 | 7.532 | 0.884 |
| Hypersharpening Synthesized | 2.878 | 7.234 | 0.923 |
| Improved Hypersharpening Synthesized | 2.469 | **6.108** | **0.941** |

Table IV: Quality indices of the vegetated sub-image.

[2] ——, "Hyper-sharpening: A first approach on SIM-GA data," *IEEE Journal of Selected Topics in Applied Earth Observations and Remote Sensing*, vol. 8, no. 6, pp. 3008–3024, 2015.

[3] A. Garzelli, L. Capobianco, L. Alparone, B. Aiazzi, S. Baronti, and M. Selva, "Hyperspectral pansharpening based on modulation of pixel spectra," in *Proceedings of the 2nd Workshop on Hyperspectral Image and Signal Processing: Evolution in Remote Sensing (WHISPERS)*, 2010, pp. 1–4.

[4] R. C. Hardie, M. T. Eismann, and G. L. Wilson, "MAP estimation of hyperspectral image resolution enhancement using an auxiliary sensor," *IEEE Transactions on Image Processing*, vol. 13, no. 9, pp. 1174–1184, September 2004.

[5] M. T. Eismann and R. C. Hardie, "Hyperspectral resolution enhancement using high-resolution multispectral imagery with arbitrary response functions," *IEEE Trans. Geosci. Remote Sensing*, vol. 43, no. 3, pp. 455–465, Mar. 2005.

[6] Y. Zhang, S. De Backer, and P. Scheunders, "Noise-resistant wavelet-based bayesian fusion of multispectral and hyperspectral images," *IEEE Transactions on Geoscience and Remote Sensing*, vol. 47, no. 11, pp. 3834–3843, 2009.

[7] N. Yokoya, T. Yairi, and A. Iwasaki, "Coupled nonnegative matrix factorization unmixing for hyperspectral and multispectral data fusion," *IEEE Transactions on Geoscience and Remote Sensing*, vol. 50, no. 2, pp. 528–537, Feb. 2012.

[8] N. Yokoya and A. Iwasaki, "Hyperspectral and multispectral data fusion mission on hyperspectral imager suite (hisui)," *International Geoscience and Remote Sensing Symposium (IGARSS)*, pp. 4086–4089, 2013.

[9] Q. Wei, N. Dobigeon, and J.-Y. Tourneret, "Bayesian fusion of hyperspectral and multispectral images," *ICASSP, IEEE International Conference on Acoustics, Speech and Signal Processing - Proceedings*, pp. 3176–3180, 2014.

[10] M. Simoes, J. Bioucas-Dias, L. Almeida, and J. Chanussot, "A convex formulation for hyperspectral image superresolution via subspace-based regularization," *IEEE Transactions on Geoscience and Remote Sensing*, vol. 53, no. 6, pp. 3373–3388, 2015.

[11] C. Kwan, B. Budavari, A. C. Bovik, and G. Marchisio, "Blind quality assessment of fused worldview-3 images by using the combinations of pansharpening and hypersharpening paradigms," *IEEE Geoscience and Remote Sensing Letters*, vol. 14, no. 10, pp. 1835–1839, Oct 2017.

[12] C. Paris, J. Bioucas-Dias, and L. Bruzzone, "A hierarchical approach to superresolution of multispectral images with different spatial resolutions," in *2017 IEEE International Geoscience and Remote Sensing Symposium (IGARSS)*, July 2017, pp. 2589–2592.

[13] J. Yang, Y.-Q. Zhao, and J. C.-W. Chan, "Hyperspectral and multispectral image fusion via deep two-branches convolutional neural network," *Remote Sensing*, vol. 10, no. 5, 2018.

[14] N. Yokoya, C. Grohnfeldt, and J. Chanussot, "Hyperspectral and multispectral data fusion: A comparative review of the recent literature," *IEEE Geoscience and Remote Sensing Magazine*, vol. 5, no. 2, pp. 29–56, 2017.

[15] B. Aiazzi, S. Baronti, and M. Selva, "Improving component substitution Pansharpening through multivariate regression of MS+Pan data," *IEEE Transactions on Geoscience and Remote Sensing*, vol. 45, no. 10, pp. 3230–3239, October 2007.

[16] G. Vivone, R. Restaino, and J. Chanussot, "A regression-based high-pass modulation pansharpening approach," *IEEE Transactions on Geoscience and Remote Sensing*, vol. 56, no. 2, pp. 984–996, Feb 2018.

[17] R. Carlà, L. Santurri, B. Aiazzi, and S. Baronti, "Full-scale assessment of pansharpening through polynomial fitting of multiscale measurements," *IEEE Transactions on Geoscience and Remote Sensing*, vol. 53, no. 12, pp. 6344–6355, 2015.

[18] M. Schaepman, M. Jehle, A. Hueni, P. D'Odorico, A. Damma, J. Weyermann, F. Schneider, V. Laurent, C. Popp, F. Seidel, K. Lenhard, P. Gege, C. Kchler, J. Brazile, P. Kohler, L. De Vos, K. Meuleman, R. Meynart, D. Schlpfer, M. Kneubhler, and K. Itten, "Advanced radiometry measurements and earth science applications with the airborne prism experiment (APEX)," *Remote Sensing of Environment*, vol. 158, no. 1, pp. 207–219, 2015.

[19] B. Aiazzi, L. Alparone, S. Baronti, A. Garzelli, and M. Selva, "MTF-tailored multiscale fusion of high-resolution MS and Pan imagery," *Photogramm. Eng. Remote Sens.*, vol. 72, no. 5, pp. 591–596, May 2006.

[20] G. Vivone, M. Simes, M. D. Mura, R. Restaino, J. M. Bioucas-Dias, G. A. Licciardi, and J. Chanussot, "Pansharpening based on semiblind deconvolution," *IEEE Transactions on Geoscience and Remote Sensing*, vol. 53, no. 4, pp. 1997–2010, April 2015.

[21] M. Selva, L. Santurri, and S. Baronti, "On the use of the expanded image in quality assessment of pansharpened images," *IEEE Geoscience and Remote Sensing Letters*, vol. PP, no. 99, pp. 1–5, 2018.

[22] Z. Wang and A. C. Bovik, "A universal image quality index," *IEEE Signal Processing Lett.*, vol. 9, no. 3, pp. 81–84, Mar. 2002.

[23] T. Ranchin and L. Wald, "Fusion of high spatial and spectral resolution images: the ARSIS concept and its implementation," *Photogramm. Eng. Remote Sens.*, vol. 66, no. 1, pp. 49–61, Jan. 2000.